Research Article Vol. 27, No. 15 | 22 Jul 2019 | OPTICS EXPRESS 20358

Optics EXPRESS

Ring-core fiber with negative curvature structure supporting orbital angular momentum modes

Jiajing Tu,[1,2,3] Zhengyong Liu,[4,7] Shecheng Gao,[1] Zhuo Wang,[2,3] Jianbo Zhang,[2,3] Bin Zhang,[5] Jianping Li,[6] Weiping Liu,[1] Hwayaw Tam,[4] Zhaohui Li,[5] Changyuan Yu,[2,3,8] and Chao Lu[2,3]

[1] *Department of Electronic Engineering, School of Information Science and Technology, Jinan University, Guangzhou 510632, China*
[2] *Department of Electronic and Information Engineering, The Hong Kong Polytechnic University, Hong Kong, China*
[3] *The Hong Kong Polytechnic University Shenzhen Research Institute,Shenzhen 518057, China*
[4] *Department of Electrical Engineering, The Hong Kong Polytechnic University, Hong Kong, China*
[5] *State Key Lab Optoelectric Material and Technology, School of Electric and Information Technology, Sun Yat Sen University, Guangzhou 510275, China*
[6] *Guangdong Provincial Key Laboratory of Optical Fiber Sensing and Communications, Institute of Photonics Technology, Jinan University, Guangzhou 510632, China*
[7] *zhengyong.liu@connect.polyu.hk*
[8] *changyuan.yu@polyu.edu.hk*

Abstract: Compared to glass walls with a positive curvature, those with a negative curvature have been proven to have stronger confinement of light. Therefore, we change the multi-layered air holes in a photonic crystal fiber into several negative curvature tubes. As a result, the confinement medium is shifted from a low-index cladding material into a special structure. The theoretical analysis shows that each vector eigenmode has a corresponding threshold value for the outer tube thickness. It means that we can confine the target modes and filter the unnecessary modes by shifting the outer tube thickness. After substantial investigation on this fiber, we obtain the appropriate values for each structural parameter and then fabricate this negative curvature ring-core fiber under the guidance of the simulation results. Firstly, we draw the central cane under vacuum condition, then stack the cane and six capillaries to form the preform, and finally draw the ring-core fiber by using vacuumization method. The fiber test experiment indicates that the fiber length should be at least 15 m~20 m to form the donut facula, and the tested losses of $OAM_{+1,1}$, $OAM_{+2,1}$, $OAM_{+3,1}$, and $OAM_{+4,1}$ are 0.30 dB/m, 0.36 dB/m, 0.37 dB/m, and 0.42 dB/m, respectively.

1. Introduction

Currently, space division multiplexing (SDM) and mode division multiplexing (MDM) are considered as promising technologies for increasing the transmission capacity of optical fiber communication systems under the continuously growing requirement for bandwidth resources [1–3]. As one of the SDM applications, multi-core fibers (MCFs), in which several cores are deployed in a particular core arrangement, have been intensively investigated [4–6]. In MCF, the cores should be arranged in a limited space of cladding with the required core-to-core distance to prevent inter-core crosstalk. Therefore, the core number cannot be increased infinitely, and it is hard to scale up this kind of fiber due to the complex core arrangement. Compared to MCF, MDM which is utilized by few-mode fiber (FMF), is a more integrated solution [7, 8]. However,

#363982 https://doi.org/10.1364/OE.27.020358
Journal © 2019 Received 2 Apr 2019; revised 31 May 2019; accepted 10 Jun 2019; published 9 Jul 2019

the modes propagated in the traditional FMF are linear polarized (LP) modes. Because LP modes consist of degenerated vector eigenmodes with different propagation constants, the inter-mode dispersion phenomenon caused by walk-off transmission can appear easily. Moreover, there would inevitably be a strong mode-coupling issue for FMF with increase in LP mode number, and a complex multiple-input-multiple-output digital signal processing (MIMO-DSP) algorithm is required to deal with the strong mode-coupling. As a result, the time and hardware/software cost brought by MIMO-DSP becomes non-negligible for MDM systems.

The orbital angular momentum (OAM) mode formed by the even and odd modes of the same vector eigenmode can be considered as a good solution to realize a MIMO-free MDM transmission without inter-mode dispersion. The OAM beam is a helically phased beam, which consists of an azimuthal phase term $\exp(il\phi)$, where l is the topological charge and ϕ is the azimuthal angle [9, 10]. Most of the previously reported OAM fibers have a ring-core structure with an annular index profile, which matches the annular electrical field distribution of the OAM mode and suppresses the high radial order mode [11–14]. Those fibers also have high refractive index contrast between the different vector eigenmodes ($> 10^{-4}$) to avoid the formation of LP modes due to the near-degeneracy of the adjacent eigenmodes. In order to achieve a large refractive index contrast between the ring-core and cladding, several up-doping air-core fibers have been proposed [11, 12]. C. Brunet *et. al* presented an optical fiber with an air core and annular index profile, which supports 9 orders of OAM modes and was fabricated by using the MCVD process [11]. P. Gregg *et. al* adopted an up-doping air-core fiber to obtain a very large refractive index contrast between the ring-core and cladding to form a strongly-guiding fiber [12]. It was demonstrated that this fiber can propagate 3 orders of OAM states (12 OAM modes) over 10 m at 1530 nm. However, the complex up-doping process and precise control of the relatively thin ring-core makes the fiber fabrication process difficult [14]. Besides the up-doing fibers, several ring-core OAM fibers based on the photonic crystal structure have been proposed [15–18]. Photonic crystal fibers (PCFs) with a hexagonal lattice is the traditional structure, but they can only support a few OAM modes due to the unsatisfactory OAM mode quality caused by the non-circular core profile. Therefore, circular type PCFs have been proposed to support a large number of OAM modes with good quality [15, 17, 18], and their cross-section is as shown in Fig. 1(a). However, it is hard to form the capillaries in a circular arrangement during the stacking process because they will eventually form a hexagonal shape due to the interaction force between them, which indicates that this circular type PCF structure needs to be improved. A. Tandjè *et. al* fabricated a PCF with hexagonal structure, where a close-to-circular ring-core with smaller air-hole are made in the center, and this fiber was proved to support OAM modes [19]. Besides this method, we can also change the confinement medium from a low-index cladding material into a special structure. The circular type PCF shown in Fig. 1(a) can be equivalent to a Bragg fiber with a one-dimensional transverse periodicity of concentric rings as shown in Fig. 1(b), if the relative air-hole diameter becomes very large. It has been reported that negatively curved glass walls have stronger confinement of light than positively curved ones, and this was proved by Y. Wang *et. al* [20]. They compared the loss performance of multi-layered annular fibers and negative curvature fibers, and the results for fibers with four interfaces are shown in Fig. 1(c), where the radius of the air-core (a), the distance of the tube (d), and the thickness of the tube (t) in the annular fiber are 15 μm, 10 μm, and 0.24 μm, respectively and the radius of the air-core (a'), the distance of the tube (d'), and the thickness of the tube (t') in the negative curvature fiber are 14.33 μm, 16 μm, and 0.24 μm, respectively [20]. Hence, a similar fiber with negative curvature structure, as shown in Fig. 1(d), can be proposed to support a large number of OAM modes and achieve ultra-low loss for the higher order modes.

Here, we propose a new type of ring-core fiber with negative curvature tubes to support OAM modes. In the ring-core, all the modes are confined by the total internal reflection (TIR), and the light confinement can be enhanced by the Fresnel reflection from the outside negative curved

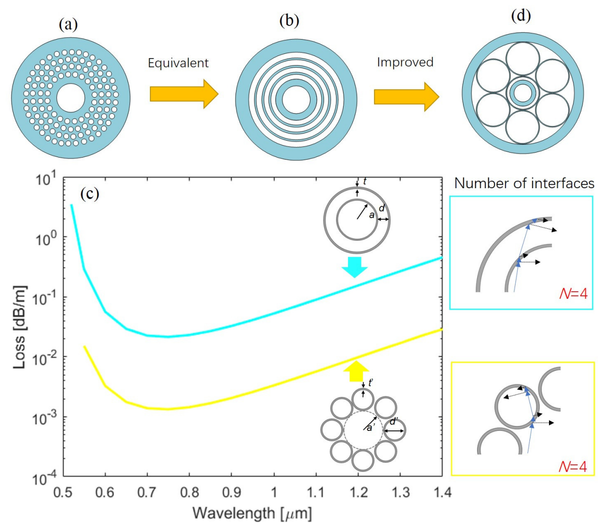

Fig. 1. (a)Circular type photonic crystal fiber, (b) equivalent Bragg fiber, (c) loss comparison between multi-layered annular fiber and negative curvature fiber, where the radius of the air-core (a), the distance of the tube (d), and the thickness of the tube (t) in the annular fiber are 15 μm, 10 μm, and 0.24 μm, respectively, and the radius of the air-core (a'), the distance of the tube (d'), and the thickness of the tube (t') in the negative curvature fiber are 14.33 μm, 16 μm, and 0.24 μm, respectively, and (d) improved ring-core fiber with negative curvature tubes.

glass wall, which is also known as the anti-resonant effect. We will explain the design process, introduce the OAM modes control method, and finally present the fabricated fiber.

2. Fiber design and fabrication

The cross-section of the proposed negative curvature ring-core fiber (NC-RCF) is shown in Fig. 2, where r_0 and r are the inner and outer radii of the ring-core, respectively, d and Λ are the inner diameter of the air hole and the distance between the adjacent air holes, respectively, t and R are the thickness and inner radius of the cladding tubes, respectively, and D is the outer diameter of the fiber. In this simulation work, the tube outside the air-hole has the same thickness as that of the six outer cladding tubes, which is also denoted by t. All the simulation results are obtained through the finite element method (FEM) by using the commercial software COMSOL.

Designing fiber involves figuring out how the structural parameters affect the fiber properties

(a)

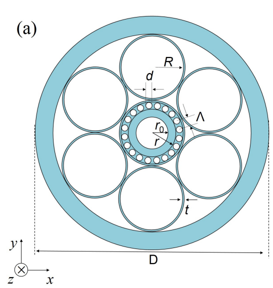

(b)

Parameter	Description
r_0	inner radius of the ring-core
r	outer radius of the ring-core
ρ (r_0/r)	ratio of annular radii of the ring core
d	diameter of the air-hole
Λ	Air-hole pitch
d/Λ	relative air-hole diameter
t	Thickness of tube
R	Radius of tube
D	Outer diameter of the substrate
λ/Λ	normalized wavelength

Fig. 2. (a) Cross-section of the proposed negative curvature ring-core fiber (NC-RCF), and (b) description of each structural parameter.

and then deciding the design region for each parameter based on the target function of the fiber. For the proposed NC-RCF, the structural parameters include core index (n_{co}), cladding index (n_{cl}), wavelength (λ), thickness of the ring-core, and thickness of the cladding tube (t). Here, n_{co}, n_{cl}, and λ can be summarized in the effective normalized frequency (V_{eff}), while the thickness of the ring-core can be normalized as the ratio of the inner radius to the outer radius ($\rho = r_0/r$). Therefore, the design steps for this NC-RCF are as follows: A. decide the expression of V_{eff} by analyzing the corresponding n_{cl} for different air-hole sizes and wavelengths; B. investigate how V_{eff}, ρ, and t influence the fiber properties and then decide the design region for these parameters; C. present the fiber characteristics, such as the separation degree between the vector eigenmodes in one OAM group, that between adjacent OAM groups, confinement loss, bending loss, nonlinear efficient, and chromatic dispersion.

2.1. Expression of the effect normalized frequency V_{eff}

Normalized frequency plays an important role in evaluating the propagation characteristics of a fiber, because it includes the fundamental structure parameters of the fiber. The effective normalized frequency (V_{eff}) of this proposed fiber is expressed as

$$V_{eff} = \frac{2\pi}{\lambda} r \sqrt{n_{co}^2 - n_{cl}^2}, \tag{1}$$

where λ is the operating wavelength, n_{co} is the core index (which is set as 1.444), and n_{cl} is the cladding index. For this NC-RCF with a special cladding structure, n_{cl} is an unknown parameter. The relative hole diameter (d/Λ) and the normalized wavelength (λ/Λ) are two key values for deciding the cladding index n_{cl}. First, we obtain the effective index (n_{eff}) of the NC-RCF for different d/Λ and λ/Λ. Figure 3(a) shows the calculated n_{eff} of the NC-RCF as a function of λ/Λ with d/Λ ranging from 0.2 to 0.8 in steps of 0.1, where r and r_0/r are set to be 7 μm and 0.6, respectivley. Subsequently, we calculate the corresponding cladding index of the step index ring-core fiber (SI-RCF) as shown in Fig. 3(b) for each n_{eff} in Fig. 3(a), and this SI-RCF has the same ring-core size as that of NC-RCF. Figure 3(c) shows the n_{cl} dependence on λ/Λ with d/Λ ranging from 0.2 to 0.8 in steps of 0.1, and this cladding index can be approximately treated as that of the NC-RCF. After getting the n_{cl}, the V_{eff} values for each d/Λ and λ/Λ can be obtained. The fitting curves are shown in Fig. 3(d), and the fitting equation is given by Eq. (2). In Eq. (2), the fitting parameters A_i (i = 1 to 3) depend on d/Λ only. The data are well described by Eq. (3), and the coefficients a_i to d_i are given in Table 1. According to Eq. (2) and Eq. (3), we can easily understand the V_{eff} value of the NC-RCF.

$$V_{eff}(\tfrac{\lambda}{\Lambda}, \tfrac{d}{\Lambda}) = A_1(\tfrac{d}{\Lambda}) \ln(\tfrac{d}{\Lambda})^2 + A_2(\tfrac{d}{\Lambda}) \ln(\tfrac{d}{\Lambda}) + A_3(\tfrac{d}{\Lambda}), \tag{2}$$

$$A_i(\tfrac{d}{\Lambda}) = a_i(\tfrac{d}{\Lambda})^3 + b_i(\tfrac{d}{\Lambda})^2 + c_i(\tfrac{d}{\Lambda}) + d_i. \tag{3}$$

Table 1. Fitting coefficients in Eq. (3).

-	a_i	b_i	c_i	d_i
i=1	-10.95	22.62	-12.8	2.11
i=2	-13.25	31.29	-27.68	-0.4285
i=3	-4.75	-2.625	15.75	4.335

Optics EXPRESS

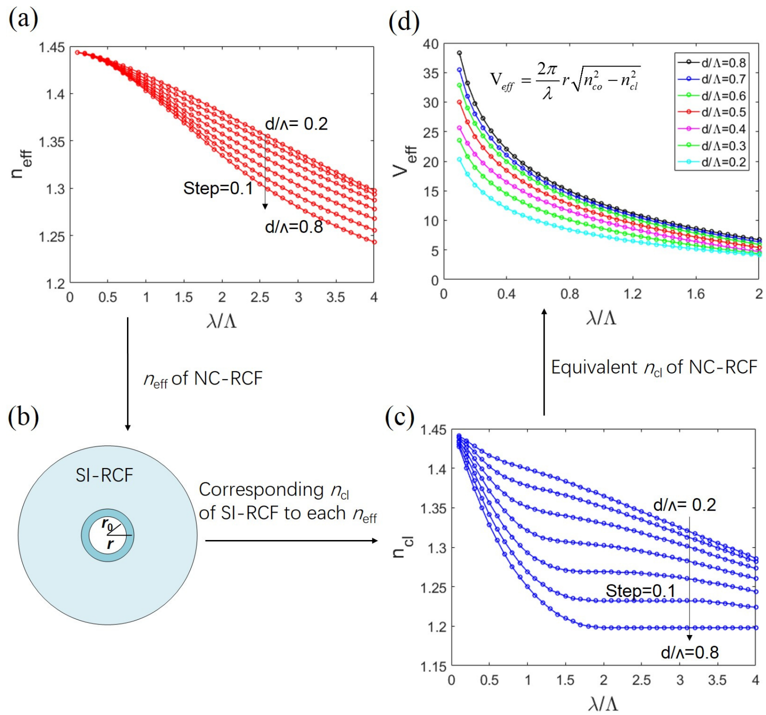

Fig. 3. (a) n_{eff} of NC-RCF as a function of λ/Λ, where $r = 7$ μm and $r_0/r = 0.6$, (b) cross-section of step-index ring-core fiber (SI-RCF) with the same r and r_0 as that of NC-RCF, (c) corresponding n_{cl} of SI-RCF for each n_{eff} in (a), and (d) V_{eff} as a function of d/Λ and λ/Λ.

2.2. Cutoff condition for OAM modes

The OAM modes are formed by a linear combination of the vector eigenmodes with $\pm\pi/2$ phase shift, which can be expressed as

$$\begin{bmatrix} \sigma^+ OAM_{+l,m} \\ \sigma^- OAM_{-l,m} \\ \sigma^- OAM_{+l,m} \\ \sigma^+ OAM_{-l,m} \end{bmatrix} = F_{l,m} \begin{bmatrix} 1 & i & 0 & 0 \\ 1 & -i & 0 & 0 \\ 0 & 0 & 1 & i \\ 0 & 0 & 1 & -i \end{bmatrix} \begin{bmatrix} HE^{even}_{l+1,m} \\ HE^{odd}_{l+1,m} \\ EH^{even}_{l-1,m} \\ EH^{odd}_{l-1,m} \end{bmatrix}, \quad (4)$$

where σ^+ and σ^- represent the left and right circular polarization, respectively, $F_{l,m}$ is the radial field distribution, l denotes the topological charge number, m is the radial order, which indicates the intensity profile of the mode in the radial direction, the sign $+/-$ in front of l indicates the right or left rotation of the wavefront, and i represents a $\pi/2$ phase shift. When $l = 0$, the $\sigma^{\pm}\text{OAM}_{\pm 0,m}$ mode is formed by the combination of two fundamental modes $\text{HE}_{1,m}$ with left or right circular polarization, but it cannot be treated as an OAM mode since they carry no OAM [11]. For $l = 1$, OAM has two states, $\sigma^{\pm}\text{OAM}_{\pm 1,m}$ mode, which is composed of $\text{HE}^{even}_{2,m}$ and $\text{HE}^{odd}_{2,m}$ with the same directions of polarization and wavefront rotation. When $l > 1$, 4 OAM states can be obtained.

To decide the OAM mode number, we firstly investigate the cutoff condition of each vector eigenmode. Besides the above-mentioned V_{eff}, the ratio of the inner radius to the outer radius

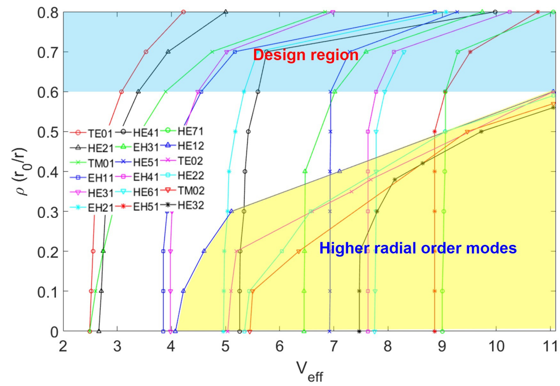

Fig. 4. Cutoffs of each vector eigenmode as a function of V_{eff} and ρ with $d/\Lambda = 0.8$.

of ring-core ρ (in other words, the thickness of the ring-core) also has a significant impact on the OAM characteristics. Figure 4 illustrates the cutoff condition of V_{eff} and ρ for each vector eigenmode, where $d/\Lambda = 0.8$. In order to ensure the quality of the OAM modes, the higher radial order modes should be suppressed, because the phase distributions of higher radial order modes ($m > 1$) are different at different areas of different rings, which makes the multiplexing and demultiplexing of OAM modes very difficult. This fact indicates that m of OAM should be 1. As shown in Fig. 4, ρ should be at least larger than 0.6 to prevent higher radial order modes. However, the thickness of the ring core cannot be reduced infinitely, because it is hard for the very thin ring core to support the OAM modes with good quality. After considering this trade-off, the range of ρ is set to be 0.6~0.8, which is shown as the blue area in Fig. 4, while the selected V_{eff} depends on the target number of OAM modes.

However, when V_{eff} becomes larger than 11, ρ of > 0.6 is not enough to suppress the higher

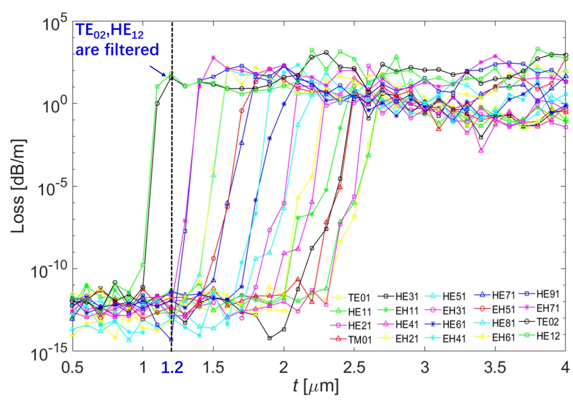

Fig. 5. Dependence of confinement loss on t where $r = 7$ μm, $\rho = 0.65$, $\lambda = 1.55$ μm, and $d/\Lambda = 0.8$.

radial order mode any more. Fortunately, there is another way to control the OAM modes, that is, controlling the thickness of the outer negative curvature cladding tubes t. Figure 5 shows the dependence of the confinement loss (CL) of each vector eigenmode on t, where $r = 7$ μm, $\rho = 0.65$, $\lambda = 1.55$ μm, and $d/\Lambda = 0.8$. For each vector eigenmode, there is a threshold value of t to make the light confinement condition of the negative curvature tubes change from anti-resonance

Optics EXPRESS

to resonance. It means that the mode number can be controlled and some specified modes can be filtered by tuning the parameter t. Here, t of 1.2 μm is the critical value that can filter the higher radial order modes TE_{02} and HE_{12} while confining the OAM component vector eigenmodes HE_{21}, $HE_{l+1,1}$ and $EH_{l-1,1}$ ($i = 2, 3, 4, 5, 6, 7, 8$). Moreover, we also calculate the surface scattering loss (SSL) based on the expressions in [21, 22] and the estimated SSL is about 10^{-4} dB/m. Thus, we can conclude that if t is smaller than the threshold value, the SSL is the dominated loss, while when t becomes larger than the threshold value, the CL becomes the dominated one. Here, t of 1.2~2.5 μm can be regarded as an appropriate design region for the designed NC-RCF.

In order to prove the effect of those negative curvature tubes, we investigated four cases with

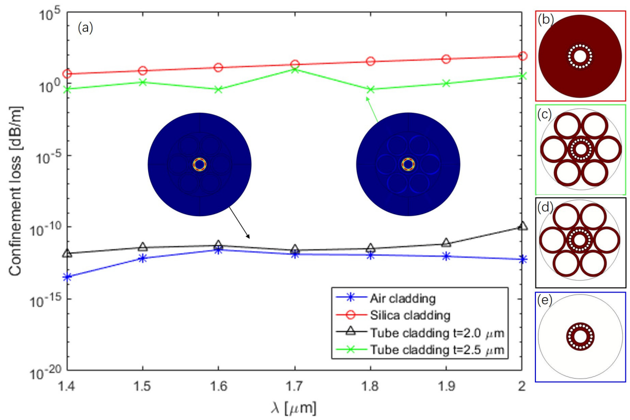

Fig. 6. (a) Dependence of the confinement loss on the wavelength for (b) silica cladding model, (c) negative curvature tube cladding with t=2.0 μm, (d) negative curvature tube cladding with t=2.5 μm and (e) air cladding model.

different cladding materials or structures, which are 1) silica cladding, 2) air cladding, 3) negative curvature tube cladding with t=2.0 μm, and 4) negative curvature tube cladding with t=2.5 μm. Figures 6(a) illustrates the calculated confinement loss for these four cases, which are shown in Figs. 6(b)-6(e). In these Figs. 6(b)-6(e), red color represents the silica and white color represents the air. In Fig. 6(a), the red and blue lines illustrate the confinement losses of HE_{31} mode for ring-core fiber with silica cladding and air cladding, respectively. Since the refractive index of air is much lower than that of the silica, the air cladding helps the ring-core fiber obtain the ultra-low confinement loss. The green and black lines in Fig. 6(a) show the confinement losses of ring-core fiber with negative curvature tubes when t=2.5 μm, and t=2.0 μm, respectively. It is obvious that the thickness of the negative curvature tubes has very big impact on the confinement of mode. When t is 2.0 μm, the confinement degree of negative curvature tubes is very close to the air cladding, however, when t is increased to be 2.5 μm, there is an obvious increase in the confinement loss. This phenomenon can be explained by the mode coupling and anti-resonant effect. When t=2.0 μm, the thickness of the negative curvature tube makes the ring-core fiber work under the anti-resonant condition and the mode in the core will not be coupled out into the tubes, which can be illustrated by the electrical field distribution of HE_{31} mode shown at the left side of Fig. 6(a). However, when t= 2.5 μm, anti-resonance and inhibited coupling condition of the tubes have been broken, the ring-core fiber works in the resonant status and a lot of energy are coupled into the tubes, which can be understood by observing the electrical field distribution of HE_{31} mode shown at the right side of Fig. 6(a). Therefore, it has been proven that the negative curvature structure is a good cladding candidate to further confine the mode.

Research Article | Vol. 27, No. 15 | 22 Jul 2019 | OPTICS EXPRESS 20365
Optics EXPRESS

2.3. Characteristics of OAM mode

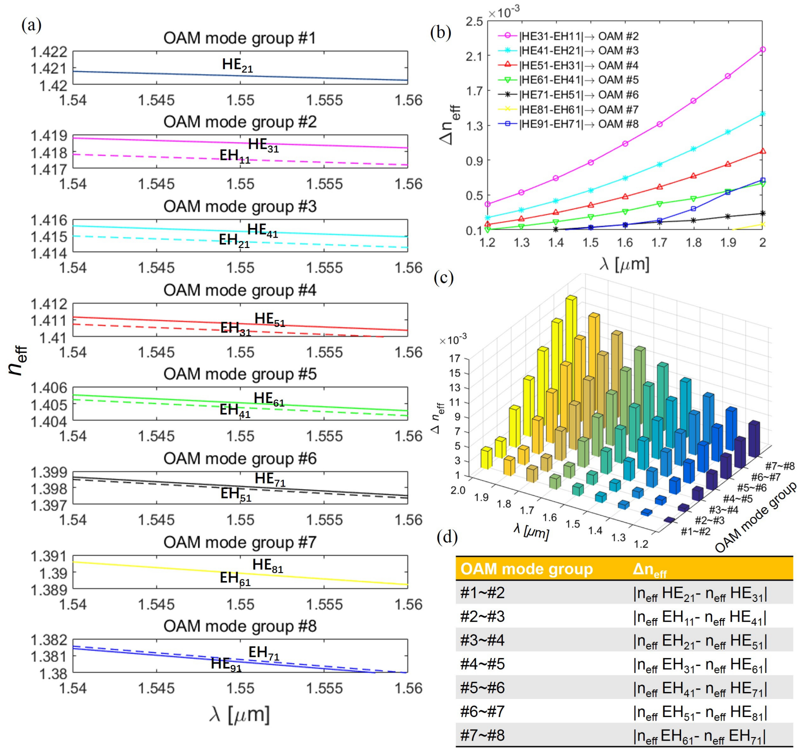

OAM mode group	Δn_{eff}
#1~#2	$\lvert n_{eff}\,HE_{21} - n_{eff}\,HE_{31}\rvert$
#2~#3	$\lvert n_{eff}\,EH_{11} - n_{eff}\,HE_{41}\rvert$
#3~#4	$\lvert n_{eff}\,EH_{21} - n_{eff}\,HE_{51}\rvert$
#4~#5	$\lvert n_{eff}\,EH_{31} - n_{eff}\,HE_{61}\rvert$
#5~#6	$\lvert n_{eff}\,EH_{41} - n_{eff}\,HE_{71}\rvert$
#6~#7	$\lvert n_{eff}\,EH_{51} - n_{eff}\,HE_{81}\rvert$
#7~#8	$\lvert n_{eff}\,EH_{61} - n_{eff}\,EH_{71}\rvert$

Fig. 7. (a) Dependence of n_{eff} on λ, where $r = 7$ μm, $\rho = 0.65$, $t = 1.2$ μm, and $d/\Lambda = 0.8$, (b) Δn_{eff} between the adjacent vector eigenmodes in each OAM mode group, (c) minimum Δn_{eff} between OAM mode groups, and (d) accurate modes used to calculate the minimum Δn_{eff} in (c) .

For the designed NC-RCF, we take V_{eff} of 17.5 as an example to discuss the fiber properties. In the simulation, $r = 7$ μm, $\rho = 0.65$, $t = 1.2$ μm, and $d/\Lambda = 0.8$. In order to ensure that the HE and EH vector modes are not coupled into the LP mode again, Δn_{eff} should be larger than 10^{-4}, which is the modal birefringence of the polarization-maintaining fibers. Therefore, we investigate the n_{eff} of each vector eigenmode and calculate the value of Δn_{eff}. Figure 7(a) shows the dependence of n_{eff} of each vector eigenmode on λ for OAM mode groups 1~8, where the solid lines and dashed lines stand for the HE mode and EH mode, respectively. It is obvious that the gap between the HE mode and EH mode in an OAM mode group reduces as the order of the OAM mode group increases. Figure 7(b) shows the dependence of Δn_{eff} between the adjacent vector eigenmodes in an OAM mode group on λ. It is seen that the Δn_{eff} between HE mode and EH mode in OAM mode groups #2, #3, #4, #5, #6, #8 can meet the requirement of > 1×10^{-4} in the wavelength band 1.4~1.8 μm. Figure 7(c) illustrates the minimum Δn_{eff} between the adjacent OAM mode groups over λ from 1.2~2.0 μm. The accurate modes used to calculate the minimum Δn_{eff} between the OAM mode groups are summarized in the table shown in Fig. 7(d). In Fig. 7(c), it can be found that the n_{eff} gap between OAM mode groups increases as the order of the OAM mode group increases, which is the opposite trend to that observed for the Δn_{eff} between HE mode and EH mode in one OAM mode group. As λ increases, the n_{eff} gap between OAM mode groups will also increase and all the Δn_{eff} between OAM mode groups become larger than

Optics EXPRESS

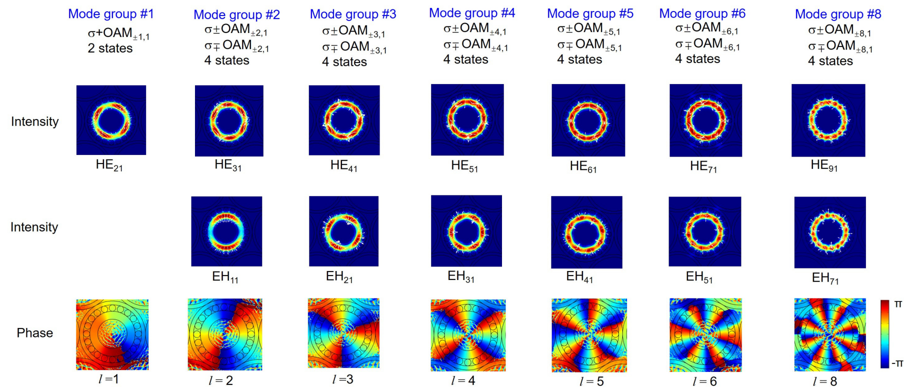

Fig. 8. Mode intensity distribution and electric field distribution for vector eigenmodes in OAM mode groups #1, #2, #3, #4, #5, #6, and #8.

$1{\times}10^{-3}$ when $\lambda > 1.2$ μm. Therefore, the proposed NC-RCF can theoretically support 26 OAM states in the telecommunication band as follows: OAM mode group #1 (2 states), #2 (4 states), #3 (4 states), #4 (4 states), #5 (4 states), #6 (4 states), and #8 (4 states). The mode intensity distribution, electric field distribution, and phase are all included in Fig. 8.

Subsequently, we analyze the different fiber characteristics, such as confinement loss, bending loss, nonlinear efficiency (γ), and chromatic dispersion (CD). Here, confinement loss is expressed by Eq. (5) in unit of dB/m, and the imaginary part of the effective index is obtained by adding a perfect match layer (PML) to the fiber model in COMSOL. In Eq. (5), k is the wavenumber in vacuum and $k = 2\pi/\lambda$. The bending loss is calculated by using the equivalent refractive index, which is expressed by Eq. (6). The parameters γ and CD are given by Eq. (7) and Eq. (8), respectively. In Eq. (7), n_2 is the nonlinear index for fused silica and is set as $2.6{\times}10^{-20}$ $\mathrm{m^2W^{-1}}$, and A_{eff} represents the effective area. In Eq. (8), c and n_{eff} are the velocity of light in vacuum and the effective index, respectively. Firstly, we swept the wavelength and confinement loss spectra of the 13 vector eigenmodes are shown in Fig. 9(a). From Fig. 9(a), we can find that all the modes have ultra-low confinement loss, thanks to the anti-resonant effect of the outer cladding tubes, and if λ is larger than about 1.64 μm, the losses of HE_{91} and EH_{71} increase immediately due to that the longer wavelength breaks the anti-resonance condition and light cannot be suppressed anymore. Figure 9(b) shows the bending loss dependence on the bending radius (R_c) at λ of 1.55 μm, and it is known that the bending loss vibrates only slightly when R_c is changing. Figure 9(c) and 9(d) illustrate the γ and CD characteristics over the C+L wavelength bands. In Fig. 9(c) and Fig. 9(d), we can find that γ is within 1.3~1.8 over the C+L bands, which is close to that of a single-mode fiber, and the CD curves are significantly flattened with a maximum dispersion slope of 0.2051 ps/(km$\cdot$ nm^2) (HE_{91}).

$$Loss = 8.686kIm(n_{\mathrm{eff}}), \tag{5}$$

$$n(x,y) = n_0(x,y)(1 + x/R_c), \tag{6}$$

$$\gamma = \frac{2\pi n_2}{\lambda A_{\mathrm{eff}}}, \tag{7}$$

$$CD = -\frac{\lambda}{c}\frac{d^2 Re(n_{\mathrm{eff}})}{d\lambda^2}. \tag{8}$$

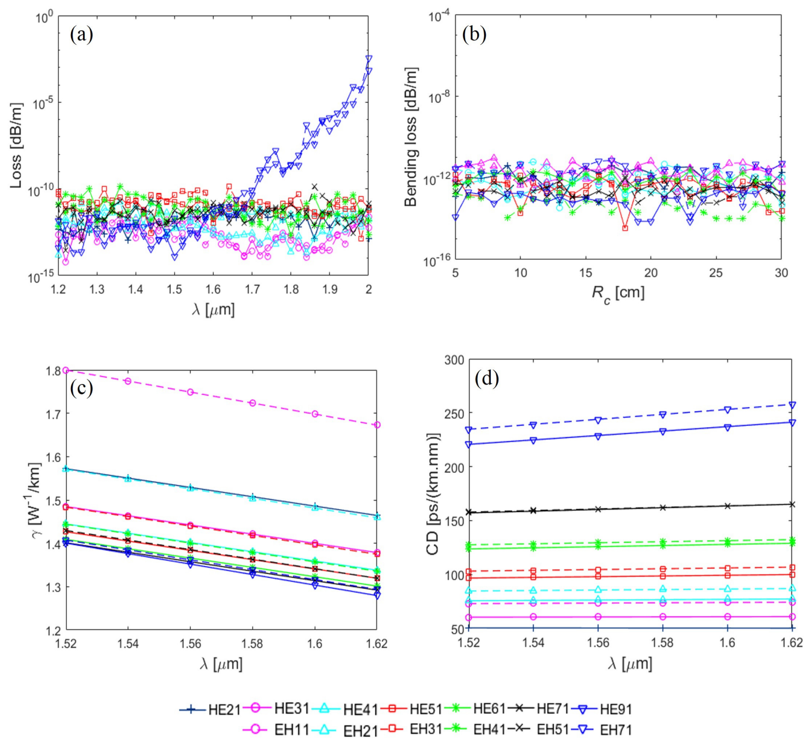

Fig. 9. (a) Dependence of confinement loss on λ, (b) dependence of bending loss on R_c, where λ is 1.55 μm, (c) nonlinear coefficient γ over C+L bands, and (d) chromatic dispersion over C+L bands.

2.4. Fabrication

Figure 10(a) shows the fabrication process of the NC-RCF, where two drawing stages were utilised to fabricate the designed fiber. This included four steps: 1) stack the center preform, 2) draw the center cane, 3) stack the fiber preform, 4) draw the fiber. In the first step, we used two types of fused silica tubes and 21 identical capillaries to stack the structure of the central ring-core. The inner and outer diameters of these silica tubes and capillaries are shown as tube ①, tube ②, and capillary ③ in Tab. 2. One end of tube ① and that of capillaries ③ were sealed before stacking. The sealed capillaries and preform of the central ring-core are shown in Fig. 10(b) and 10(c), respectively. In the second step, the stacked preform with the structure of the central ring-core was drawn to a cane with a diameter of ~1.3 mm, which is named as cane ⑤, under vacuum; its microscopic cross-section is shown in Fig. 10(d). In the third step, six capillaries ③ and one of the canes were sealed at one end and then stacked in tube ④ to obtain the second preform, as shown in Fig. 10(f). Finally, the second stacked preform was drawn to the fiber with an outer diameter of ~125 μm under vacuum of 60 kPa. The drawing temperature was about 1880 °C, which is relatively lower than that used for drawing an all-solid fiber to maintain the structure. Figure 10(g) shows the cross-sectional scanning electron microscopic (SEM) photo of the drawn fiber.

Figure 11 shows the enlarged views of the fabricated fiber shown in Fig. 10(g). From Fig. 11, we can find that the ring-shape of the core is maintained very well, which is important to support OAM modes. From the SEM photos, the inner and outer radius of the ring-core were measured as r_0 = ~4.5 μm, and r = ~6.6 μm, respectively. The ratio of the inner radius to the outer radius of

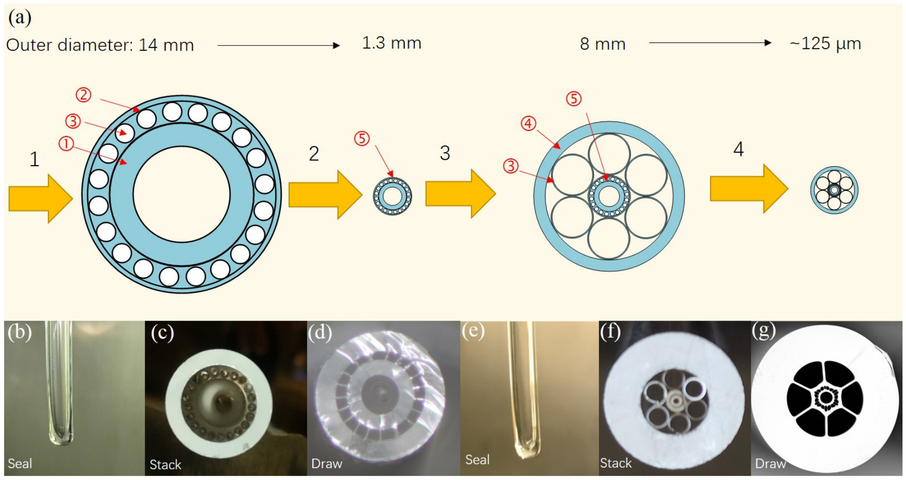

Fig. 10. Fabrication of the proposed negative curvature ring-core fiber (NC-RCF). (a) Schematic figure of the fabrication process using stack-and-draw approach. In the first step, stack the preform of the central ring-core with outer diameter of 14mm; in the second step, draw the stacked preform to a cane with outer diameter of 1.3 mm; in the third step, stack the preform of the NC-RCF in an 8 mm tube, where the cane is placed in the center; in the fourth step, draw the preform to the designed fiber with outer diameter of 125 μm. (b) Sealed capillaries for the first stack. (c) Stacked preform of the central cane. (d) Cross section of the intermedia cane. (e) Sealed capillaries for second stack. (f) Stacked preform of the NC-RCF. (g) Scanning electron microscopic photo of the fabricated NC-RCF.

Table 2. The inner diameters and outer diameters of the silica tubes and capillaries used in the fabrication process.

-	Inner diameter [mm]	Outer diameter [mm]
Tube ①	4	7
Tube ②	10	14
Capillary ③	1.1	1.29
Tube ④	4	8

the ring core is ρ = ~0.68, and relative air-hole size is d/Λ = ~0.78. These structural parameters of the fabricated fiber are in good agreement with the designed values used in the simulation, where r_0 = 4.55 μm, r = 7 μm, ρ = 0.65, and d/Λ = 0.8. Since the fiber was drawn with vacuum, the gaps between the adjacent outer tubes collapsed, resulting in slightly different values from that of the design. However, the negative curvature structures were formed successfully and the anti-resonant effect still confines the light. The characterization of the fabricated NC-RCF and its confinement capacity of OAMs are discussed in the following section.

3. Results and discussion

Figure 12 shows the experimental setup used to verify the transmission of OAM modes through the fabricated NC-RCF. At the input end, an erbium-doped fiber amplifier (EDFA) is used to increase the light power of the external cavity laser (ECL, 1550nm, 6 dBm) to 25.5 dBm. An

Optics EXPRESS

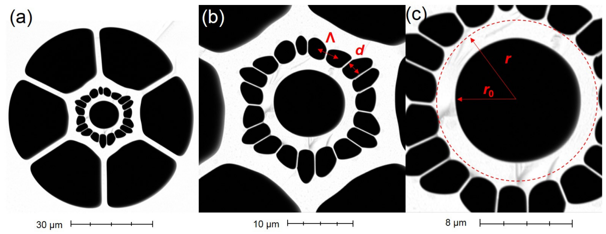

Fig. 11. Enlarged views of the fabricated fiber, with scale lengths of (a) 30 μm, (b) 10 μm, and (c) 8 μm.

optical coupler (99:1) is connected to the EDFA, splitting the light into two branches: one is for OAM generation and the other one transmits directly to the end via SMF. The OAM mode generated by the SLM is coupled to the NC-RCF by a lens (L) with a focal length of 25.4 mm. At the receiver end, we use an objective lens (OL, 40/0.65, 160/0.17) to collect the light. Clear interference patterns were observed on the CCD by combining the two outputs from NC-RCF and SMF (the inputted OAM beam profile and interference pattern of $OAM_{+1,1}$ are shown in Fig. 12), thereby proving the OAM propagation of the fabricated NC-RCF. We also conducted four sets of experiments with different fiber lengths (3 m, 15 m, 20 m, and 40 m) to observe the facula. The beam profiles of $OAM_{+1,1}$, $OAM_{+2,1}$, $OAM_{+3,1}$, and $OAM_{+4,1}$ after propagating 3 m, 15 m, 20 m, and 40 m are illustrated in Figs. 13(a-1)-13(a-4), Figs. 13(b-1)-13(b-4), Figs. 13(c-1)-13(c-4), and Figs. 13(d-1)-13(d-4), respectively. When the fiber is 3 m, two layers of facula can be found in Figs. 13(a-1), 12(b-1), 12(c-1), and 12(d-1) due to the thick outer layer of silica around the ring-core, which also confines the light. With the increase in fiber length, the outer layer of the facula fades gradually, as illustrated in Figs. 13(a-2)-13(a-4), Figs. 13(b-2)-13(b-4), Figs. 13(b-2)-13(b-4), and Figs. 13(b-2)-13(b-4). The disappearance of the outer facula indicates that the light in the outer layer is not coupled from the central ring-core, and the suppression of the outer facula is due to the high bending loss of the light propagating in the outer layer. In the experiment, fiber length of about 15 m~20 m was used to suppress the outer ring effect completely. To verify the propagation of OAM modes in the fabricated NC-RCF, further simulation was carried out by sketching the actual structure of the fiber cross section. The results are shown in Fig. 13 for comparison. The simulated intensity profiles agree well with the measured ones, and the phase indicates the orders of the OAM modes.

The propagation loss of OAM in the fabricated fiber was measured by using the cut-back method. Taking OAM mode with $l = +1$ as an example, after the $OAM_{+1,1}$ was coupled into the NC-RCF, we adjusted the position of the fiber very slightly to obtain the highest coupling power and recorded the output power (P1). Subsequently, we cut a 5 m-long fiber and then recorded the output power (P2) without changing the launching condition. Hence, the propagation loss of this NC-RCF can be calculated via 10log(P1/P2)/5 (dB/m). Since the fiber length of the fabricated NC-RCF is limited and proper length of the fiber remains at the input side to guarantee a single layer of facula, we only test the losses of the first four OAM modes by using 40 m NC-RCF with banding radius of ~8 cm. The losses of $OAM_{+1,1}$, $OAM_{+2,1}$, $OAM_{+3,1}$, and $OAM_{+4,1}$ were 0.30 dB/m, 0.36 dB/m, 0.37 dB/m, and 0.42 dB/m, respectively.

We also compare the fiber properties for the reported ring-core fibers and the proposed negative curvature ring-core fiber. Although the measured loss of the fiber in this experiment is relative high compared to the other fabricated ring-core fibers, the novel principle of confining mode still have the potentiality to obtain lower loss and large mode separation. In the next fabrication, we will try the best to make the silica layer outside the air-hole thinner and thus enhance the confinement.

Optics EXPRESS

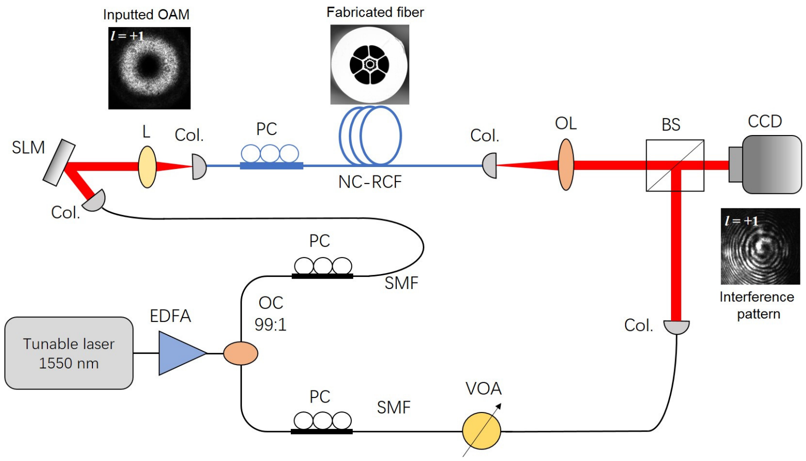

Fig. 12. Experimental setup for the generation and transmission of OAM through NC-RCF.EDFA: erbium-doped fiber amplifier; OC: optical coupler; PC: polarization controller; SMF: single mode fiber; Col.: collimator; SLM: spatial light modulator; L: lens; NC-RCF: negative curvature ring-core fiber; OL: objective lens; BS: beam splitter; CCD: charge coupled device; VOA: variable optical attenuator.

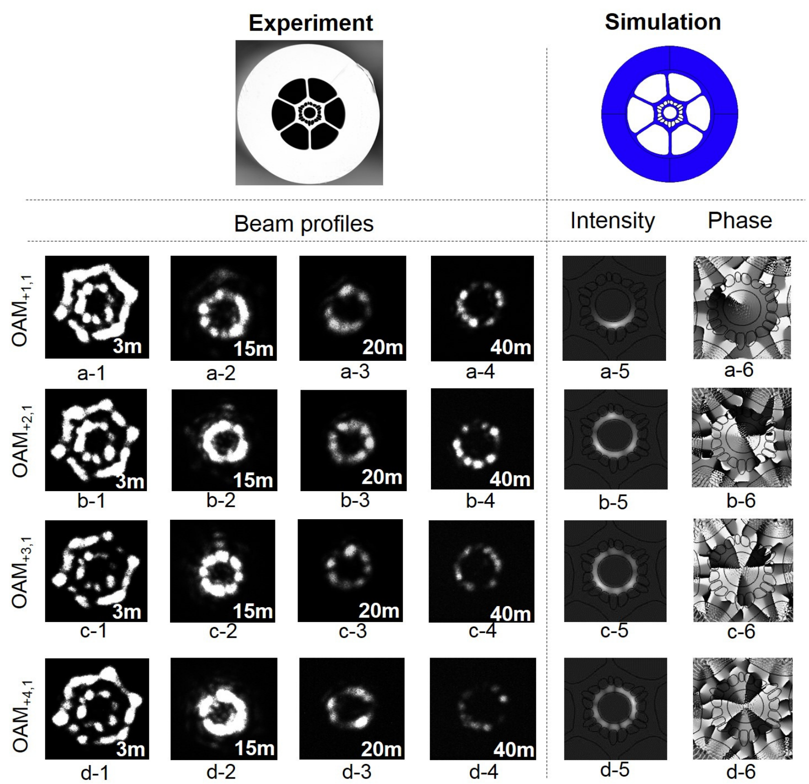

Fig. 13. Experiment results: beam profiles for (a) $OAM_{+1,1}$, (b) $OAM_{+2,1}$, (c) $OAM_{+3,1}$, and (d) $OAM_{+4,1}$ when fiber length is 3 m, 15 m, 20 m, and 40 m; simulation results: intensity and phase for (a) $OAM_{+1,1}$, (b) $OAM_{+2,1}$, (c) $OAM_{+3,1}$, and (d) $OAM_{+4,1}$.

Optics EXPRESS

Table 3. Comparison among the reported ring-core fibers and the proposed negative curvature ring-core fiber in this work.

Ring-core fiber type	Simulation		Experiment	
	OAM mode order	Min $\Delta n_{\mathrm{eff}}(1.55\mu m)$	OAM mode order	Measured loss($1.55\mu m$)
Up-doping [11]	-	$\sim 0.2\times 10^{-3}$	2	6.5dB/km(l=1)
Up-doping [12]	3	$\sim 0.1\times 10^{-3}$	3	2.2dB/km(l=6)
Circular PCF [18]	7	$\sim 0.5\times 10^{-3}$	-	-
Circular PCF [15]	11	$\sim 0.2\times 10^{-3}$	-	-
Hexagonal PCF [19]	4	$\sim 0.7\times 10^{-3}$	2	50 dB/km(total)
Negative curvature(this work)	7	$\sim 0.2\times 10^{-3}$	4	0.3 dB/m(l=1)

4. Conclusion

We have designed and fabricated a negative curvature ring-core fiber that supports OAM modes. We have given the design method for each structural parameter, including ring-core size, ring-core thickness, relative air-hole diameter, and thickness of the outer tubes. Based on the design method, appropriate values for these parameters were decided and the analysis of the fiber characteristics was presented. Thanks to the negative curvature of the outer tubes, the theoretical distinguishing feature of this NC-RCF is that the modes can be confined or filtered by adjusting the thickness of the outer tubes. For the fabricated NC-RCF, the fiber length should be at least 15 m~20 m to ensure a single layer of beam profile, and the losses of $OAM_{+1,1}$, $OAM_{+2,1}$, $OAM_{+3,1}$, and $OAM_{+4,1}$ were 0.30 dB/m, 0.36 dB/m, 0.37 dB/m, and 0.42 dB/m, respectively.

Funding

National Natural Science Foundation of China (NSFC) (U1701661); State Key Laboratory of Advanced Optical Communication Systems Networks, China.

References

1. T. Morioka, “New generation optical infrastructure technologies: ’EXAT initiative’ towards 2020 and beyond,” in *Proceeding of the 14th OptoElectronics and Communication Conference (OECC),* (HongKong, China, 2009), pp. 1–2.
2. D. Richardson, J. Fini, and L. Nelson, “Space division multiplexing in iptical fibres,” Nat. Photon. **7**, 354–362 (2013).
3. S. Matsuo, Y. Sasaki, I. Ishida, K. Takenaga, K. Saitoh, and M. Koshiba, “Recent progress on multi-core fiber and few-mode fiber,” in *Proceeding of the Optical Fiber Communication Conference (OFC),* (Anaheim, USA, 2013), pp. 1–3.
4. K. Saitoh and S. Matsuo, “Multicore fiber technology,” J. Light. Technol. **34**, 55–66 (2016).
5. J. Tu, K. Saitoh, M. Koshiba, K. Takenaga, and S. Matsuo, “Design and analysis of large-effective-area heterogeneous trench-assisted multi-core fiber,” Opt. Express **20**, 15157–15170 (2012).
6. T. Hayashi, T. Taru, O. Shimakawa, T. Sasaki, and E. Sasaoka, “Design and fabrication of ultra-low crosstalk and low-loss multi-core fiber,” Opt. Express **19**, 16576–16592 (2011).
7. P. Sillard, M. Bigot-Astruc, and D. Molin, “Few-mode fibers for mode-division multiplexed systems,” J. Light. Technol. **32**, 2824–2829 (2014).
8. R. Ryf, S. Randel, A. H. Gnauck, C. Bolle, A. Sierra, S. Mumtaz, M. Esmaeelpour, E. C. Burrows, R. J. Essiambre, P. J. Winzer, D. W. Peckham, A. H. McCurdy, and R. Lingle, “Mode-division multiplexing over 96 km of few-mode fiber using coherent 6 ×6 mimo processing,” J. Light. Technol. **30**, 521–531 (2012).
9. A. M. Yao and M. J. Padgett, “Orbital angular momentum: origins, behavior and applications,” Adv. Opt. Photon. **3**, 161–204 (2011).
10. N. Bozinovic, Y. Yue, Y. Ren, M. Tur, P. Kristensen, H. Huang, A. E. Willner, and S. Ramachandran, “Terabit-scale orbital angular momentum mode division multiplexing in fibers,” Science **340**, 1545–1548 (2013).
11. C. Brunet, P. Vaity, Y. Messaddeq, S. LaRochelle, and L. A. Rusch, “Design, fabrication and validation of an oam fiber supporting 36 states,” Opt. Express **22**, 26117–26127 (2014).

Optics EXPRESS

12. P. Gregg, P. Kristensen, and S. Ramachandran, "Conservation of orbital angular momentum in air-core optical fibers," Optica **2**, 267–270 (2015).
13. B. Ung, P. Vaity, L. Wang, Y. Messaddeq, L. A. Rusch, and S. LaRochelle, "Few-mode fiber with inverse-parabolic graded-index profile for transmission of oam-carrying modes," Opt. Express **22**, 18044–18055 (2014).
14. C. Brunet and L. A. Rusch, "Optical fibers for the transmission of orbital angular momentum modes," Opt. Fiber Technol. **35**, 2 – 7 (2017).
15. H. Zhang, X. Zhang, H. Li, Y. Deng, X. Zhang, L. Xi, X. Tang, and W. Zhang, "A design strategy of the circular photonic crystal fiber supporting good quality orbital angular momentum mode transmission," Opt. Commun. **397**, 59 – 66 (2017).
16. G. Zhou, G. Zhou, C. Chen, M. Xu, C. Xia, and Z. Hou, "Design and analysis of a microstructure ring fiber for orbital angular momentum transmission," IEEE Photonics J. **8**, 1–12 (2016).
17. Z. Hu, Y. Huang, A. Luo, H. Cui, Z. Luo, and W. Xu, "Photonic crystal fiber for supporting 26 orbital angular momentum modes," Opt. Express **24**, 17285–17291 (2016).
18. W. Tian, H. Zhang, X. Zhang, L. Xi, W. Zhang, and X. Tang, "A circular photonic crystal fiber supporting 26 oam modes," Opt. Fiber Technol. **30**, 184 – 189 (2016).
19. A. Tandjè, J. Yammine, M. Dossou, G. Bouwmans, K. Baudelle, A. Vianou, E. R. Andresen, and L. Bigot, "Ring-core photonic crystal fiber for propagation of oam modes," Opt. Lett. **44**, 1611–1614 (2019).
20. Y. Wang and W. Ding, "Confinement loss in hollow-core negative curvature fiber: A multi-layered model," Opt. Express **25**, 33122–33133 (2017).
21. F. Poletti, "Nested antiresonant nodeless hollow core fiber," Opt. Express **22**, 23807–23828 (2014).
22. L. Vincetti, "Empirical formulas for calculating loss in hollow core tube lattice fibers," Opt. Express **24**, 10313–10325 (2016).